NANO · MICRO small
www.small-journal.com

Acoustic Actuation of Integrin-Bound Microbubbles for Mechanical Phenotyping during Differentiation and Morphogenesis of Human Embryonic Stem Cells

Zhenzhen Fan, Xufeng Xue, Reshani Perera, Sajedeh Nasr Esfahani, Agata A. Exner, Jianping Fu, and Cheri X. Deng**

Early human embryogenesis is a dynamic developmental process, involving continuous and concomitant changes in gene expression, structural reorganization, and cellular mechanics. However, the lack of investigation methods has limited the understanding of how cellular mechanical properties change during early human embryogenesis. In this study, ultrasound actuation of functionalized microbubbles targeted to integrin (acoustic tweezing cytometry, ATC) is employed for in situ measurement of cell stiffness during human embryonic stem cell (hESC) differentiation and morphogenesis. Cell stiffness, which is regulated by cytoskeleton structure, remains unchanged in undifferentiated hESCs, but significantly increases during neural differentiation. Further, using the recently established in vitro 3D embryogenesis models, ATC measurements reveal that cells continue to stiffen while maintaining pluripotency during epiblast cyst formation. In contrast, during amniotic cyst formation, cells first become stiffer during luminal cavity formation, but softens significantly when cells differentiate to form amniotic cysts. These results suggest that cell stiffness changes not only due to 3D spatial organization, but also with cell fate change. ATC therefore provides a versatile platform for in situ measurement of cellular mechanical property, and cell stiffness may be used as a mechanical biomarker for cell lineage diversification and cell fate specification during embryogenesis.

Dr. Z. Fan, Prof. C. X. Deng
Department of Biomedical Engineering
University of Michigan
Ann Arbor, MI 48109, USA
E-mail: cxdeng@umich.edu
X. Xue, S. N. Esfahani, Prof. J. Fu, Prof. C. X. Deng
Department of Mechanical Engineering
University of Michigan
Ann Arbor, MI 48109, USA
E-mail: jpfu@umich.edu
Dr. R. Perera, Prof. A. A. Exner
Department of Radiology
Case Western Reserve University
Cleveland, OH 44106, USA
Prof. J. Fu
Department of Biomedical Engineering
University of Michigan
Ann Arbor, MI 48109, USA
Prof. J. Fu
Department of Cell and Developmental Biology
University of Michigan Medical School
Ann Arbor, MI 48109, USA

DOI: 10.1002/smll.201803137

During early human development, embryonic cells continue to divide, differentiate and self-organize into embryonic structures through morphogenesis. Morphogenetic events generate local mechanical perturbation and are accompanied by changes in cell shape and force, which in turn mediates cellular mechanical property changes.[1] Failure of stem cell differentiation and morphogenesis, likely associated with abnormal cellular mechanical property change, can result in abnormal embryonic or fetal development and birth defect. For example, amniotic band syndrome (ABS), which could result in limb defects, may be caused by weak mechanical property and rupture of amniotic sac.[2]

Cellular mechanical property influences stem cell fate and is also reflective of cellular stage during lineage specification and differentiation.[3–6] It may serve as a mechanical biomarker of cell phenotypes, reflecting changes, both normal and abnormal, in early development. Compared with biochemical markers, mechanical biomarkers are label-free with a great potential for in situ applications. Development of appropriate tools to characterize and track changes in cellular mechanical properties during stem cell differentiation and morphogenesis will not only help advance our knowledge of early human embryogenesis, but also establish mechanical property-based method to detect defects during human embryogenesis.

Techniques such as atomic force microscopy (AFM)[3] and magnetic twisting cytometry (MTC)[5,7] have been employed to study cellular mechanical properties. AFM provides high spatial resolution but can only perform measurements one point at a time, requires expensive equipment, and is not suitable for in situ measurements of 3D constructs. MTC is a microrheology method using functionalized magnetic microbeads attached to cells. However, solid microbeads are difficult to remove from cells, which may interfere with downstream assays that require continuous culture of cells after MTC measurements.

Acoustic tweezing cytometry (ATC), a technique we have recently developed, utilizes ultrasound pulses to actuate functionalized microbubbles attached to cell membrane proteins, such as integrin, to apply controlled subcellular mechanical

forces to cells.[8] Encapsulated microbubbles (radius 1–3 μm), typically formulated as lipid or polymer shelled gaseous microspheres,[9] are commonly used as contrast agents for clinical ultrasound imaging and have been recently utilized for other applications, including ultrasound-mediated drug and gene delivery via sonoporation.[10] Functionalization of microbubbles by decorating bubble shell with ligands to target specific cell membrane receptors has been exploited for ultrasound-based molecular imaging.[11] The periodic change of acoustic pressure of an ultrasound pulse induces volume expansion and contraction of microbubbles at the incident ultrasound frequency. Such acoustically actuated bubble activities can generate fluid microstreaming and shear stress on nearby cells, and have been exploited to probe cell deformability[12] and conduct rotational manipulation of single cells and organisms.[13] Dependent on parameters such as acoustic pressure, frequency, and microbubble radius, ultrasound field generates a net force, i.e., the primary acoustic radiation force, on a bubble. In ATC, a relatively low acoustic pressure is used to generate small volume expansion/contraction, allowing the use of the acoustic radiation force to displace an integrin-anchored microbubble from its pre-ultrasound location without bubble detachment or destruction. The displacement of integrin-anchored microbubble exerts a defined mechanical force/strain to cells via the bubble-integrin-cytoskeleton linkage. We have demonstrated that ATC can be used for applying mechanical force to elicit a variety of cellular responses such as increased cytoskeleton contractility,[8] enhanced human mesenchymal stem cell osteogenesis,[14] and rapid initiation of human embryonic stem cell differentiation.[15]

In this study, we employed ATC to assess cellular mechanical property using integrin-anchored microbubbles as a biomechanical sensor to detect changes in mechanical property of human embryonic stem cells (hESCs) during neural differentiation and early morphogenesis using a 3D in vitro model of human embryogenesis. Specifically, to measure cellular mechanical property using ATC, biotin-lipid shelled microbubbles were first conjugated with streptavidin-RGD before being attached to hESCs via RGD-integrin binding (**Figure 1**A,B). A planar ultrasound transducer (center frequency 1.25 MHz) was set at 45° angle aiming at adherent hESCs at a Rayleigh distance of 9 mm. An ultrasound pulse (duration 50 ms, acoustic pressure between 0.025 and 0.05 MPa) was applied to displace integrin-bound microbubbles on cell surface. Videomicroscopy (frame rate of 1000 frames s^{-1}) was used to record microbubble activities under ultrasound stimulations (Figure 1A). As shown in Figure 1C, a microbubble was displaced without detachment during ultrasound pulses and retracted back toward its original, pre-ultrasound location after the ultrasound pulse was turned off owing to strain recovery in the bubble-integrin-cytoskeleton linkage. The size and location of microbubbles as a function of time were extracted from recorded images and analyzed using a custom MATLAB program to determine the acoustic radiation force[16] and bubble displacement (Figure 1D). We characterized the effective cell stiffness (nN μm^{-1}) as the ratio of the acoustic radiation force exerted on the bubble (nN) to the microbubble displacement (μm).

We first investigated how the effective cell stiffness of hESCs is affected by treatment with drugs that inhibit actin polymerization (Cytochalasin D, 10×10^{-6} M), myosin II activity (Blebbistatin, 10×10^{-6} M), and RhoA/ROCK signaling (Y-27632, 10×10^{-6} M). These drug treatments perturbed cytoskeleton structure as shown by p-MYOSIN and ACTIN immunostaining (Figure 1E). The effective cell stiffness significantly decreased after drug treatments, from 6.52 ± 0.60 nN μm^{-1} (control, $n = 16$) to 3.99 ± 0.51 nN μm^{-1} (Cyto D, $n = 16$), 4.33 ± 0.44 nN μm^{-1} (Bleb, $n = 27$), and 3.75 ± 0.60 nN μm^{-1} (Y27, $n = 15$), respectively. These data are consistent with the well-established role of the cytoskeleton structure in regulating cell stiffness. When hESCs were fixed with 4% formaldehyde, which cross-links primary amino groups and thus should increase cell rigidity, cell stiffness increased from 6.52 ± 0.60 nN μm^{-1} (control, $n = 16$) to 54.28 ± 8.48 nN μm^{-1} ($n = 14$) (Figure 1F). Together, these results demonstrate that ATC can effectively detect changes in cell stiffness of hESCs due to chemical perturbations of intracellular cytoskeleton structure.

We next investigated how cell mechanical property changes during neuroepithelial cell differentiation of hESCs in a monolayer format. For control group, hESCs were cultured in mTeSR1 medium for 8 d to maintain pluripotency, which was confirmed by OCT4 staining (**Figure 2**A). Stiffness of hESCs cultured with mTeSR1 exhibited no changes during 8 d of culture, even with cell proliferation (Figure 2B). To induce neural differentiation, dual Smad inhibitors, SB 431542 (TGF-β inhibitor; 10×10^{-6} M) and LDN 193189 (BMP inhibitor; 500×10^{-9} M) were added to mTeSR1 medium. At day 8, hESCs completely differentiated into $PAX6^+$ and OCT^- neuroepithelial cells (Figure 2C). Cell stiffness during neural differentiation significantly increased in a monotonic fashion, from 6.33 ± 0.86 nN μm^{-1} ($n = 36$; day 1) to 10.56 ± 1.89 nN μm^{-1} ($n = 29$) at day 4 and 14.61 ± 2.48 nN μm^{-1} ($n = 19$) at day 8, respectively (Figure 2D). These results show that neural differentiation of hESCs resulted in increased cell stiffness, a finding that is consistent with recent studies reporting increased cell stiffness of hESCs when losing pluripotency.[17]

We have recently established a human pluripotent stem cell (hPSC)-based in vitro model for studying peri-implantation human amniotic sac development.[18] By engineering the cellular microenvironment including substrate rigidity, cell density and culture dimensionality, we have shown that hPSCs could develop into 3D epiblast cysts or amniotic cysts containing a single luminal cavity through self-organization and morphogenesis.[18] Given that mechanical property is critical for early embryogenesis and many birth defects including ABS are associated with abnormal mechanical properties of embryonic cells and tissues, we employed ATC to investigate changes in cellular mechanical property during epiblast and amniotic cyst formation using our hPSC-based in vitro model.

To generate epiblast cysts, hESCs were seeded as single cells onto a 1% Geltrex-coated glass coverslip, in mTeSR1 medium supplemented with ROCK inhibitor Y27632. On day 1 (24 h after cell seeding), culture medium was replenished with mTeSR1 medium supplemented with 4% v/v Geltrex to form a 3D extracellular matrix (ECM) overlay (**Figure 3**A). On day 2, hESCs self-organized to form columnar cysts with a single luminal cavity. Continuous development of hESC cysts increased the cyst size on day 3. Columnar cysts expressed pluripotent epiblast marker OCT4 and thus were referred as

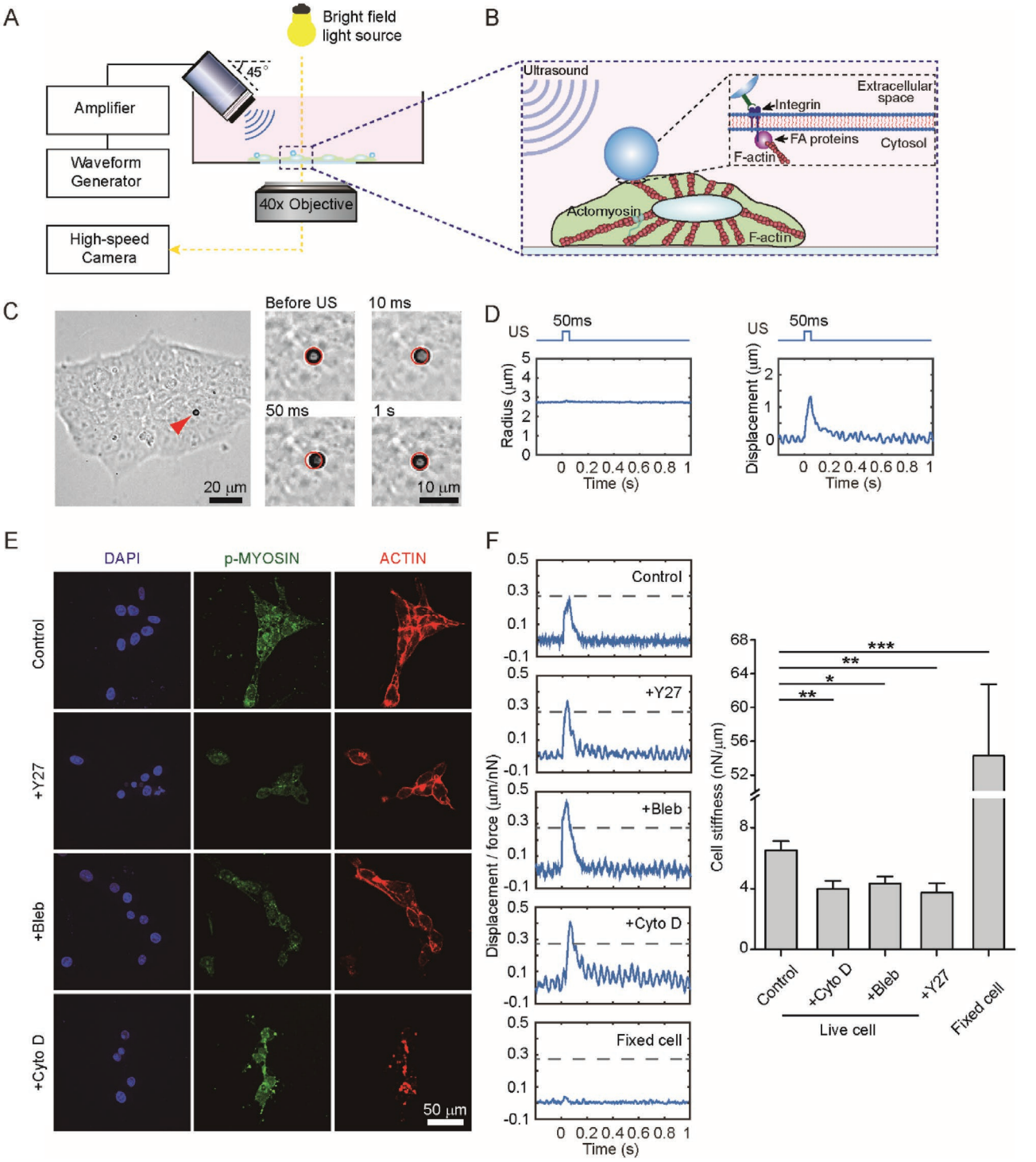

Figure 1. Application of integrin-anchored microbubble for biomechanical property sensing using acoustic tweezing cytometry (ATC). A) Schematic showing the experimental setup. B) Zoom-in illustration showing the use of targeted microbubbles attached to cells via RGD-integrin binding in ATC. C) Representative images show the integrin-bound microbubble (red arrow) in a colony before ATC, and bubble displacement during application of an ultrasound pulse (duration 50 ms). The red circle indicates the original location of the bubble before ultrasound application. The microbubble returned to its original location after ultrasound was turned off (at 1 s). D) The corresponding ultrasound pulse profile, time course of bubble radius, and bubble displacement from images shown in (C) extracted using a custom MATLAB program. E) Representative fluorescence images showing p-MYOSIN and ACTIN expression of hESCs in the control and treated groups. Treatment lasted for 2 h before ultrasound application. F) Time course of microbubble displacement divided by the acoustic radiation force of the ultrasound pulse and the effective cell stiffness as the ratio of maximum displacement to the acoustic radiation force. Error bar, mean ± SEM. *, $p < 0.05$; **, $p < 0.01$; ***, $p < 0.001$. Ultrasound parameter: center frequency 1.25 MHz, pulse duration 50 ms, acoustic pressure in the range 0.025–0.05 MPa.

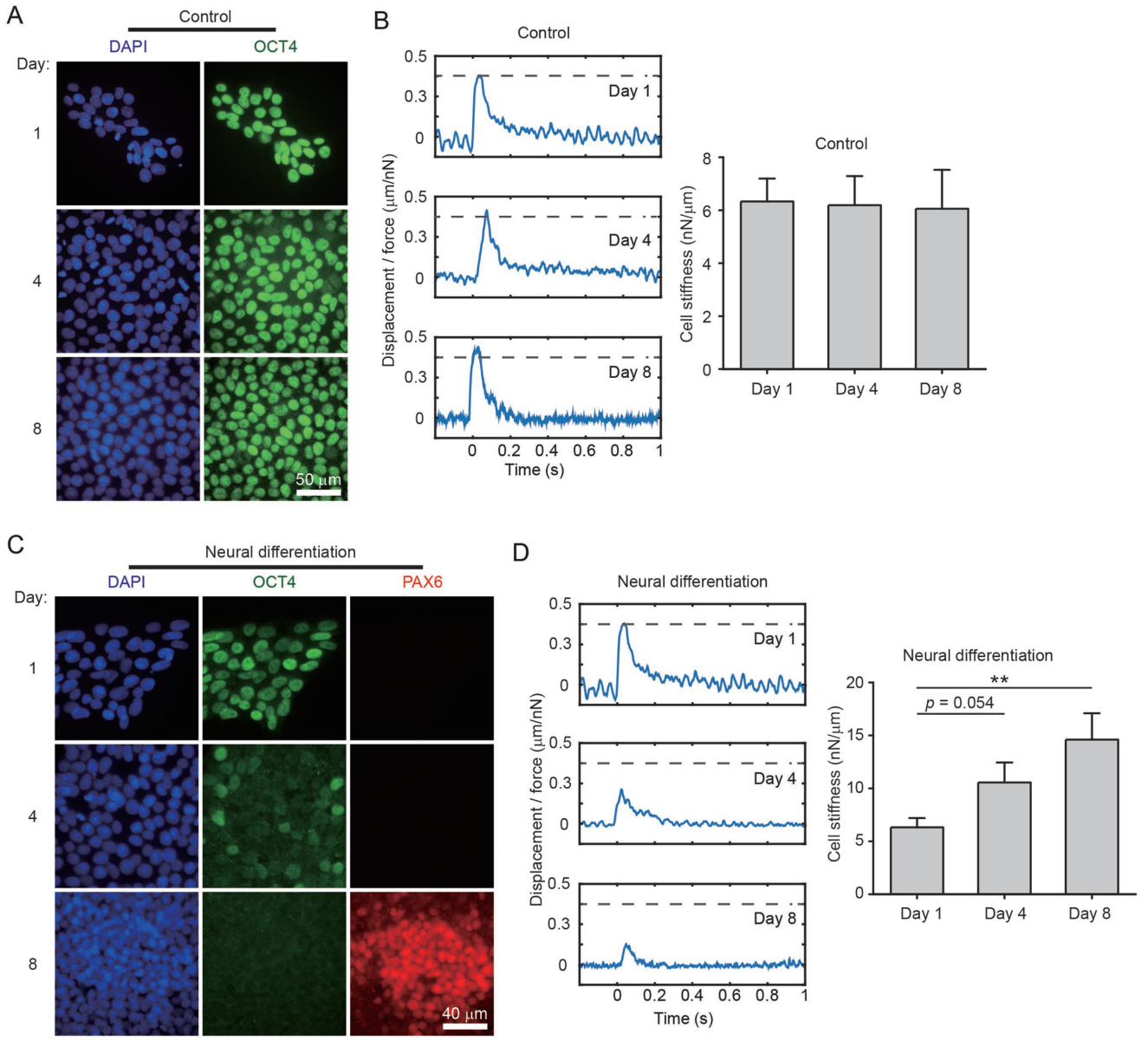

Figure 2. Cell stiffness increased during neuronal differentiation. A) Confocal micrographs showing OCT4 immunostaining in hESCs in control group. hESCs were cultured in mTeSR1 medium to maintain pluripotency. B) Representative time course of microbubble displacement divided by the acoustic radiation force of the ultrasound pulse, and the cell stiffness in control group at day 1, 4, and 8. C) Confocal micrographs of OCT4 and PAX6 immunostaining of hESCs during neural differentiation. hESCs were cultured in mTeSR1 medium supplemented with dual Smad inhibitors, SB 431542 (TGF-β inhibitor; 10×10^{-6} M) and LDN 193189 (BMP inhibitor; 500×10^{-6} M), to induce neuroepithelial cell differentiation. D) Representative time course of microbubble displacement divided by the primary acoustic radiation force of the ultrasound pulse, and the stiffness of cells cultured in neural induction medium at day 1, 4, and 8. Error bar, mean ± SEM. **, $p < 0.01$. Ultrasound parameter: center frequency 1.25 MHz, pulse duration 50 ms, acoustic pressure in the range 0.025–0.05 MPa.

epiblast cysts (Figure 3B,C). Increased ACTIN and p-MYOSIN staining intensities (Figure 3D,F) suggest stronger cytoskeleton structure as hESCs self-organized to form 3D columnar epiblast cysts. Indeed, stiffness of pluripotent hESCs in epiblast cysts on day 2 (effective cell stiffness = 10.84 ± 1.48 nN μm^{-1}, $n = 10$) and day 3 (effective cell stiffness = 10.77 ± 1.47 nN μm^{-1}, $n = 8$) was significantly higher than that of hESCs in a 2D monolayer at day 1 (effective cell stiffness = 4.84 ± 0.82 nN μm^{-1}, $n = 16$) (Figure 3E,G).

When 4% Geltrex 3D ECM overlay was applied in mTeSR1 medium 2 h after cell seeding (instead of 24 h after cell seeding), amniogenic differentiation of hESCs was triggered, leading to formation of squamous amniotic cysts on day 3 (**Figure 4**A). As amniotic cysts formed, hESCs gradually lost pluripotency, evidenced by decreased OCT4 expression and increased expression of amniotic cell marker TFAP2A over time (Figure 4B,C). Measurements of cell stiffness using ATC show that compared with

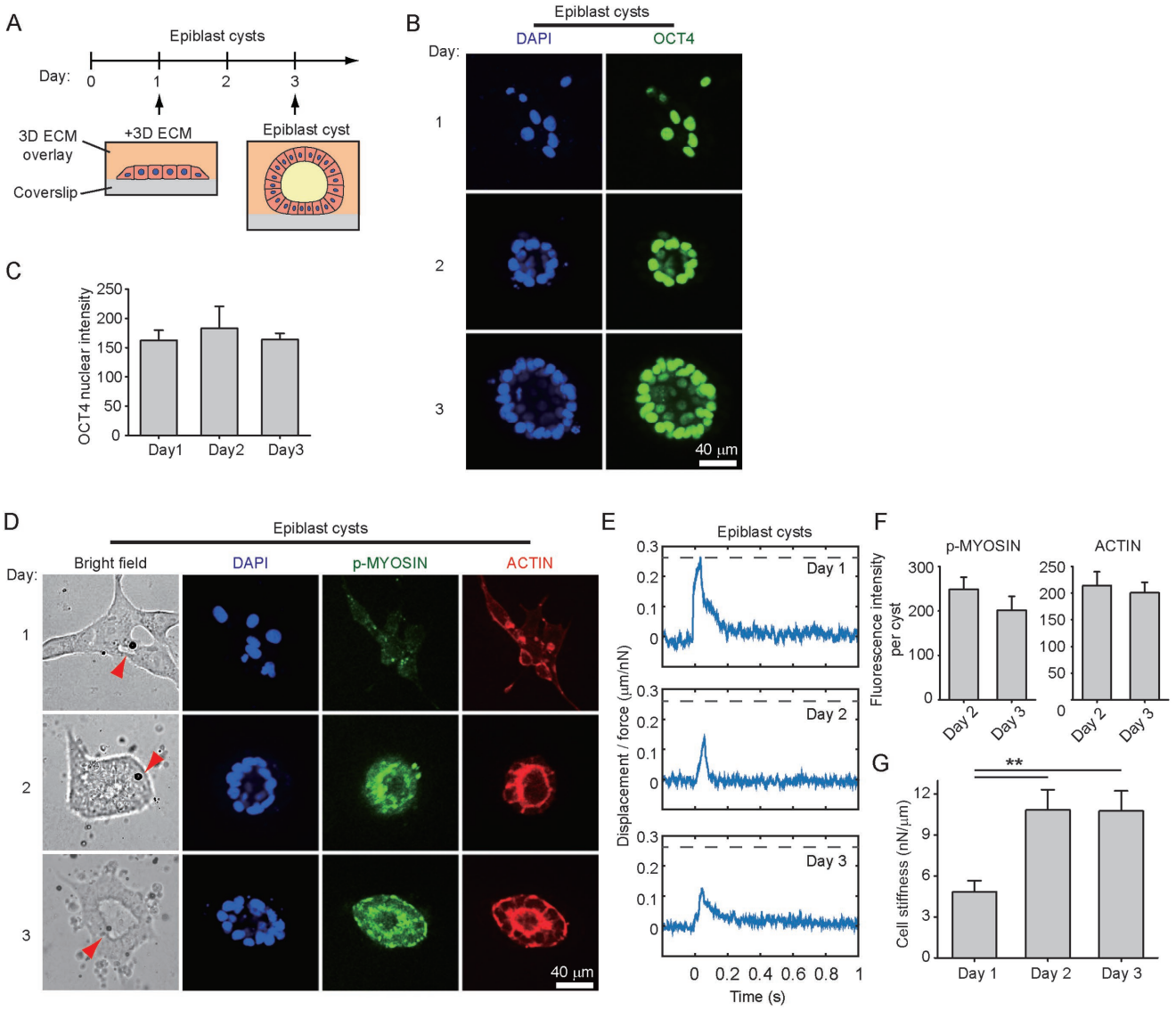

Figure 3. Cellular mechanical property changed during epiblast cyst formation. A) Schematic of the 3D culture protocol and the time line of epiblast cyst formation. B) Confocal micrographs showing OCT4 immunostaining as hESCs formed epiblast cysts. hESCs remained pluripotent as they form epiblast cyst. C) Nuclear fluorescence intensity of OCT4 of hESCs from day 1 to day 3 during epiblast cyst formation. D) Representative bright field images and confocal micrographs showing the morphology of cells during epiblast cyst formation, attachment of microbubbles (red arrows), and immunostaining of p-MYOSIN and ACTIN. E) Representative time course of microbubble displacement divided by the primary acoustic radiation force of the ultrasound pulse. F) Background subtracted total fluorescence intensity of p-MYOSIN and ACTIN per epiblast cyst on day 2 and day 3. G) The cell stiffness during epiblast cyst formation at day 1, 2, and 3. Error bar, mean ± SEM. **, $p < 0.01$. Ultrasound parameter: center frequency 1.25 MHz, pulse duration 50 ms, acoustic pressure in the range 0.025–0.05 MPa.

day 1 (cell stiffness = 8.53 ± 2.52 nN μm^{-1}, $n = 9$), cells became stiffer when forming a 3D cystic structure on day 2 before losing pluripotency and initiating amniotic differentiation program (cell stiffness = 25.46 ± 4.82 nN μm^{-1}, $n = 10$). This observation is also consistent with our finding on stiffer epiblast cysts compared with hESCs in a 2D monolayer (Figure 3). However, as pluripotent hESCs differentiated into TFAP2A$^+$ amniotic cells from day 2 to day 3 (Figure 4B,C), cells became squamous and flattened with a concomitant, significant decrease in cell stiffness (7.47 ± 1.07 nN μm^{-1}, $n = 9$) (Figure 4E,G). Consistently, cell softening during amniotic cyst development from day 2 to day 3 was accompanied by decreased ACTIN and p-MYOSIN expression levels in cystic structures (Figure 4D,F).

Further comparison of epiblast cysts and amniotic cysts obtained at day 3 shows that cell stiffness of epiblast cysts (10.77 ± 1.47 nN μm^{-1}, $n = 8$) was significantly higher than that of amniotic cysts (7.47 ± 1.07 nN μm^{-1}, $n = 9$), consistent with higher staining intensities of p-MYOSIN and ACTIN in epiblast cysts (p-MYOSIN, 201.42 ± 31.33; ACTIN, 200.50 ± 19.38, $n = 12$) than those in amniotic cysts (p-MYOSIN, 129.87 ± 20.71; ACTIN, 163.38 ± 7.77, $n = 16$).

Taken together, these results reveal several interesting and important insights. Cell stiffness remained unchanged

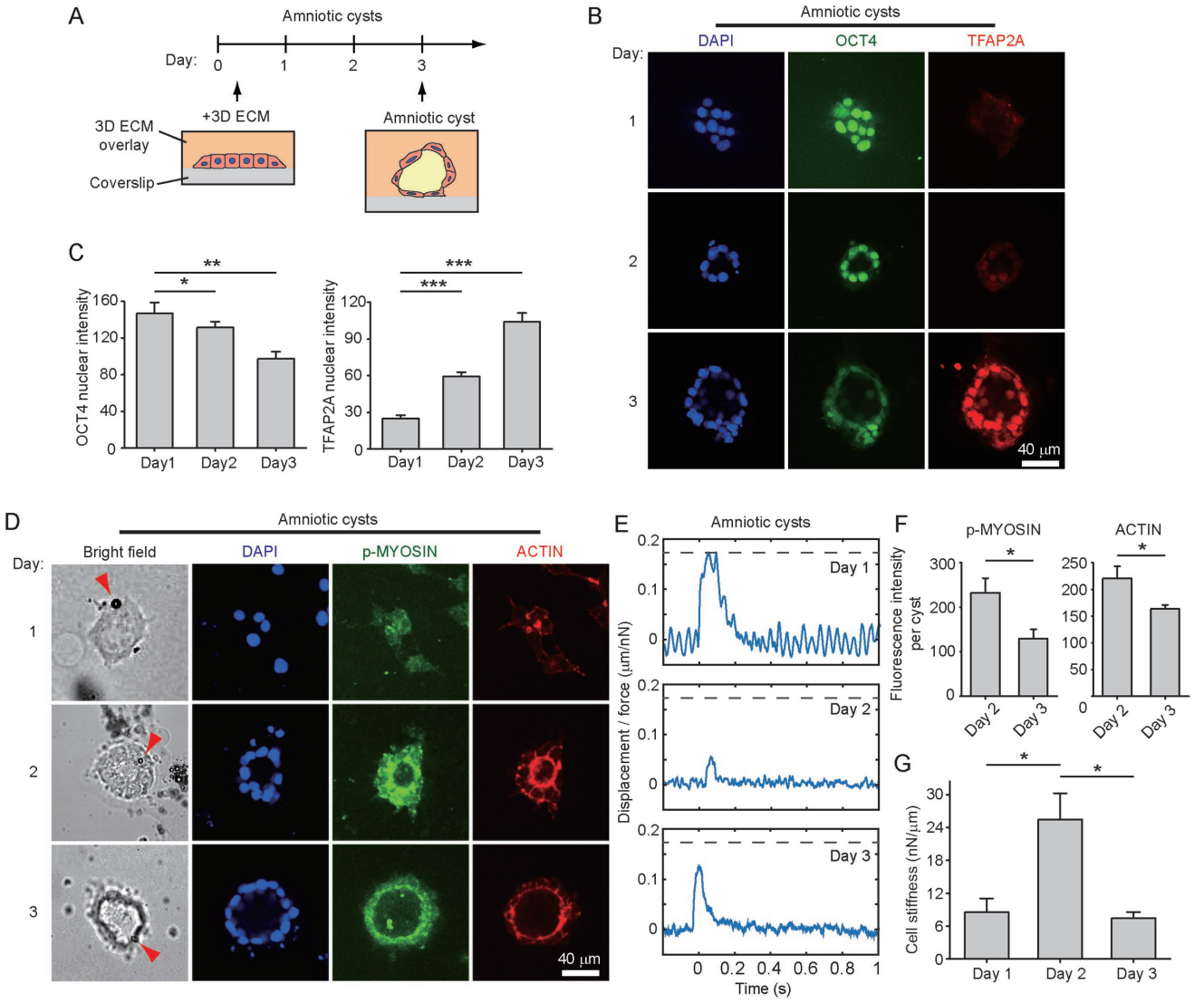

Figure 4. Change of cellular mechanical during amnion cyst formation. A) Schematic of the 3D culture protocol and the time line of amnion cyst formation. B) Confocal micrographs showing OCT4 and TFAP2A immunostaining as hESCs formed amnion cysts. C) Nuclear OCT4 and TFAP2A fluorescence intensity of cells on day 1, day 2, and day 3 during amnion cyst formation. D) Representative bright field images and confocal micrographs showing the morphology of cells during amnion cyst formation, attached microbubbles (red arrows) on the cyst, and immunostaining of p-MYOSIN and ACTIN. E) Representative time course of microbubble displacement divided by the primary acoustic radiation force of the ultrasound pulse. F) Background subtracted total fluorescence intensity of p-MYOSIN and ACTIN per amniotic cyst on day 2 and day 3. G) Cell stiffness during amnion cyst formation on day 1, 2, and 3. Error bar, mean ± SEM. *, $p < 0.05$; **, $p < 0.01$; ***, $p < 0.001$. Ultrasound parameter: center frequency 1.25 MHz and pulse duration 50 ms, acoustic pressure in the range 0.025–0.05 MPa.

for hESCs in a 2D monolayer during long-term culture, but increased significantly with spatial organization of undifferentiating hESCs into 3D epiblast cysts. Different profiles of temporal changes in cell stiffness were observed during formation of epiblast cysts and amniotic cysts from hESCs. During the development of amniotic cysts, cell stiffness would first increase at day 2 before decreasing at day 3; this biphasic change in cell stiffness was accompanied by dynamic morphogenic changes occurring concomitantly during the formation of amniotic cysts, with a columnar structure expressing OCT4 at day 2 before turning into a squamous, differentiated amniotic tissue at day 3. Together, our data support close interconnections between cell mechanics (stiffness), cell fate and lineage specification and tissue morphogenesis during embryonic development. Recent studies have further supported the role of cell mechanics, as an integral drive for morphing tissue formation, in guiding tissue-scale cell fate patterning.[6]

As we have demonstrated previously, epiblast and amniotic cyst formation are accompanied by concurrent transcriptional and morphological changes.[18] Human embryonic stem cells maintain pluripotency during epiblast cyst formation, while during amniotic cyst formation, they lose pluripotency, differentiate, and express markers associated with amniotic tissues such as TPAP2A. Morphologically, an epiblast cyst on day 3 is composed of columnar epithelial cells featuring apicobasally

elongated nuclei and a thick epithelium. In contrast, an amniotic cyst at day 3 features a squamous epithelial morphology with flattened, laterally elongated cell nuclei and a thin epithelium.[18] While it is difficult to decouple the impacts from transcriptomic and morphological perspectives on cell mechanical property, cell stiffness difference we detected in this study between epiblast cysts and amniotic cysts is likely resulted from differences in both transcriptional profiles and tissue morphology.

The epiblast and amniotic cysts we studied here are both symmetric structures derived from hESCs. Thus, cell stiffness is expected to be uniform throughout entire cystic structures, and our measurement of cell stiffness using ATC should be representative of all cells composing the cysts. For asymmetric embryonic tissues such as the asymmetric amniotic sac cyst we have reported recently,[19] cell stiffness of different cell types could be different. Since multiple microbubbles can be attached to cells at different locations on the surface of 3D tissues, we expect that the ATC method can be utilized for assessing spatial distributions of cellular mechanical properties in 3D tissue structures.

It is worth noting that the specific mode of force application in the ATC is different from other methods such as AFM. In ATC, a local mechanical force/strain is applied to cells via the bubble-integrin-cytoskeleton linkage, and the effective cell stiffness is determined as the ratio of force to microbubble displacement. In AFM, however, a local force is applied to a small area on cell surface by compression using a cantilever to determine compressive cell stiffness. It is well appreciated that different methods used for gauging cell stiffness may lead to different measurements and interpretation based on the difference in operational principles with different techniques. We should also note that during measurements of cell stiffness using the ATC, a single ultrasound pulse with a relatively short duration of 50 ms was used to displace integrin-bound microbubbles. The acoustic pressure was also chosen to minimize effects of bubble expansion and contraction or cavitation. Thus, we do not expect the ATC operation for in situ cell stiffness measurements will perturb cellular responses in culture systems being investigated.

It should also be noted that relative position of bubbles on a cell could impact the cell stiffness measurement, which may in fact contribute to the spread of measured cell stiffness presented in this study. However, we did not particularly control the relative position of bubbles on a cell, and just treated all measurements as the same. Thus, our results suggest that the cell stiffness variation associated with different bubble locations is minor compared with the change in cell stiffness that resulted from human embryonic stem cells at different developmental stages.

In conclusion, employing ATC with integrin-bound microbubbles as a versatile, biocompatible, and efficient tool for assessing in situ cellular mechanical property in both 2D and 3D structures, we obtained new results that reveal cell stiffness changes during neural differentiation and morphogenesis of hESCs. Our results support that cell stiffness measured using ATC may provide a label-free mechanical biomarker for cell lineage diversification and cell fate specification during embryogenesis.

Supporting Information

Supporting Information is available from the Wiley Online Library or from the author.

Acknowledgements

Z.F. and X.X. contributed equally to this work. This work was supported by the National Institutes of Health (R01 EB019436 and R21 EB017078 to C.X.D. and J.F., and R01 EB025741 to A.A.E.), and the National Science Foundation (CBET 1149401 to J.F.). The authors thank Dr. Yue Shao's contribution to amniogenesis assay development.

Conflict of Interest

The authors declare no conflict of interest.

Keywords

acoustic tweezing cytometry, amniotic sac, cell stiffness, human embryonic stem cells, microbubbles

Received: August 7, 2018
Revised: September 18, 2018
Published online: November 14, 2018

[1] a) T. Lecuit, P.-F. Lenne, *Nat. Rev. Mol. Cell Biol.* **2007**, *8*, 633; b) C. J. Chan, C.-P. Heisenberg, T. Hiiragi, *Curr. Biol.* **2017**, *27*, R1024.
[2] J. H. Walter, L. R. Goss, A. T. Lazzara, *J. Foot Ankle Surg.* **1998**, *37*, 325.
[3] R. D. Gonzalez-Cruz, V. C. Fonseca, E. M. Darling, *Proc. Natl. Acad. Sci. USA* **2012**, *109*, E1523.
[4] D. R. Gossett, T. Henry, S. A. Lee, Y. Ying, A. G. Lindgren, O. O. Yang, J. Rao, A. T. Clark, D. Di Carlo, *Proc. Natl. Acad. Sci. USA* **2012**, *109*, 7630.
[5] F. Chowdhury, S. Na, D. Li, Y.-C. Poh, T. S. Tanaka, F. Wang, N. Wang, *Nat. Mater.* **2010**, *9*, 82.
[6] X. Xue, Y. Sun, A. M. Resto-Irizarry, Y. Yuan, K. M. Aw Yong, Y. Zheng, S. Weng, Y. Shao, Y. Chai, L. Studer, J. Fu, *Nat. Mater.* **2018**, *17*, 633.
[7] N. Wang, J. P. Butler, D. E. Ingber, *Science* **1993**, *260*, 1124.
[8] Z. Fan, Y. Sun, C. Di, D. Tay, W. Chen, C. X. Deng, J. Fu, *Sci. Rep.* **2013**, *3*, 2176.
[9] K. Ferrara, R. Pollard, M. Borden, *Annu. Rev. Biomed. Eng.* **2007**, *9*, 415.
[10] a) Z. Fan, H. Liu, M. Mayer, C. X. Deng, *Proc. Natl. Acad. Sci. USA* **2012**, *109*, 16486; b) J. Y. Lee, D. Carugo, C. Crake, J. Owen, M. de Saint Victor, A. Seth, C. Coussios, E. Stride, *Adv. Mater.* **2015**, *27*, 5484; c) M. Bez, D. Sheyn, W. Tawackoli, P. Avalos, G. Shapiro, J. C. Giaconi, X. Da, S. B. David, J. Gavrity, H. A. Awad, H. W. Bae, E. J. Ley, T. J. Kremen, Z. Gazit, K. W. Ferrara, G. Pelled, D. Gazit, *Sci. Transl. Med.* **2017**, *9*, eaal3128.
[11] A. L. Klibanov, *J. Nucl. Cardiol.* **2007**, *14*, 876.
[12] Y. Xie, N. Nama, P. Li, Z. Mao, P. H. Huang, C. Zhao, F. Costanzo, T. J. Huang, *Small* **2016**, *12*, 902.
[13] D. Ahmed, A. Ozcelik, N. Bojanala, N. Nama, A. Upadhyay, Y. Chen, W. Hanna-Rose, T. J. Huang, *Nat. Commun.* **2016**, *7*, 11085.
[14] X. Xue, X. Hong, Z. Li, C. X. Deng, J. Fu, *Biomaterials* **2017**, *134*, 22.

[15] T. Topal, X. Hong, X. Xue, Z. Fan, N. Kanetkar, J. T. Nguyen, J. Fu, C. X. Deng, P. H. Krebsbach, *Sci. Rep.* **2018**, *8*, 12977.
[16] P. A. Dayton, K. E. Morgan, A. L. S. Klibanov, G. Brandenburger, K. R. Nightingale, K. W. Ferrara, *IEEE Trans. Ultrason. Ferroelectr. Freq. Control* **1997**, *44*, 1264.
[17] a) Y. Tan, C. W. Kong, S. Chen, S. H. Cheng, R. A. Li, D. Sun, *J. Biomech.* **2012**, *45*, 123; b) G. Ofek, V. P. Willard, E. J. Koay, J. C. Hu, P. Lin, K. A. Athanasiou, *J. Biomech. Eng.* **2009**, *131*, 061011.
[18] Y. Shao, K. Taniguchi, K. Gurdziel, R. F. Townshend, X. Xue, K. M. A. Yong, J. Sang, J. R. Spence, D. L. Gumucio, J. Fu, *Nat. Mater.* **2017**, *16*, 419.
[19] Y. Shao, K. Taniguchi, R. F. Townshend, T. Miki, D. L. Gumucio, J. Fu, *Nat. Commun.* **2017**, *8*, 208.

